2010 IEEE International Conference on Robotics and Automation
Anchorage Convention District
May 3-8, 2010, Anchorage, Alaska, USA

Toward the Set of Frictional Velocity Fields Generable by 6-Degree-of-Freedom Oscillatory Motion of a Rigid Plate

Thomas H. Vose, Paul Umbanhowar, and Kevin M. Lynch

***Abstract*— A position-dependent *asymptotic velocity field* describes the motion of point parts sliding with friction on the surface of a rigid oscillating plate. These fields can be used to perform manipulation tasks such as sensorless positioning of one or several parts simultaneously. This paper examines the set of fields $\mathcal{F}$ generated by periodic plate motions $\mathcal{M}$ that combine a single in-plane component and a single out-of-plane component that have square wave accelerations with 50% duty cycles, identical periods, and an arbitrary phase between them. By deconstructing the full map $\Pi : \mathcal{M} \to \mathcal{F}$ into three simpler maps, we expose the structure of $\mathcal{F}$ and its relationship to $\mathcal{M}$. To illustrate, we focus on particular plate motions in $\mathcal{M}$ that generate fields well approximated by polynomial functions of position with degree $n \leq 2$. Numerical simulations suggest that fields generated from plate motions with more than a single in-plane and a single out-of-plane component (all with the same period and square wave accelerations) are well approximated by linear combinations of fields in $\mathcal{F}$.**

I. INTRODUCTION

Based on a simplified dynamic model of a part sliding with Coulomb friction on an oscillating rigid plate, we have shown that the part's velocity is guaranteed to converge to an *asymptotic velocity* at each location on the plate's surface [1]. Thus, an *asymptotic velocity field*, which maps each position on the plate's surface to an asymptotic velocity, is a natural way of describing the friction-induced motion of parts sliding on a rigid six-degree-of-freedom (DoF) plate oscillating with small amplitude.

By simply changing the plate's motion, different asymptotic velocity fields can be programmed onto the plate's surface. These fields can be designed to perform a range of manipulation tasks. Fig. 1 shows a multi-exposure image of several parts moving in a `Whirlpool` field on our Programmable Parts-feeding Oscillatory Device (PPOD2) [1]. Without sensing, the field continuously reduces uncertainty in the parts' positions as they spiral toward the center of the plate. Other scenarios include fields designed to interact with a single part, e.g., to position or orient it; fields designed to interact with multiple parts, e.g., to assemble or sort them; and sequences of fields designed for compound tasks, e.g., to collect scattered parts in the center of the plate and then transport them all in a particular direction.

To understand the full range of viable manipulation tasks using a vibrating plate, we must understand the set of generable asymptotic velocity fields. This paper begins to address this issue by examining the set of fields $\mathcal{F}$ generated by plate motions $\mathcal{M}$ composed of a single in-plane component (i.e., in the horizontal plane) and a single out-of-plane component. These two components have square wave accelerations with zero mean and 50% duty cycles, identical periods, and an arbitrary relative phase between them[1]. Plate motions in $\mathcal{M}$ may seem restrictive, but simulations and experiments suggest that if the plate is driven with sinusoidal or triangle wave accelerations, the set of generable asymptotic velocity fields is approximately equivalent to $\mathcal{F}$. More significantly, simulations and experiments suggest that fields generated by plate motions with more than a single in-plane and a single out-of-plane component (all having the same period and square, triangle, or sinusoidal accelerations) are well approximated by linear combinations of fields in $\mathcal{F}$. Thus, we hypothesize that the fields in $\mathcal{F}$ form a basis that approximately spans the complete set of fields that can be generated by any plate motion whose six components (three in-plane and three out-of-plane) have the same period and square, triangle, or sinusoidal accelerations.

The key contribution of this paper is to deconstruct the map $\Pi : \mathcal{M} \to \mathcal{F}$ into three simpler maps that expose the structure of $\mathcal{F}$. The first map Π_1 takes any plate motion $M \in \mathcal{M}$ and a position $\tilde{\mathbf{r}}_{xy} \in \mathcal{R}^M$ on the plate surface for

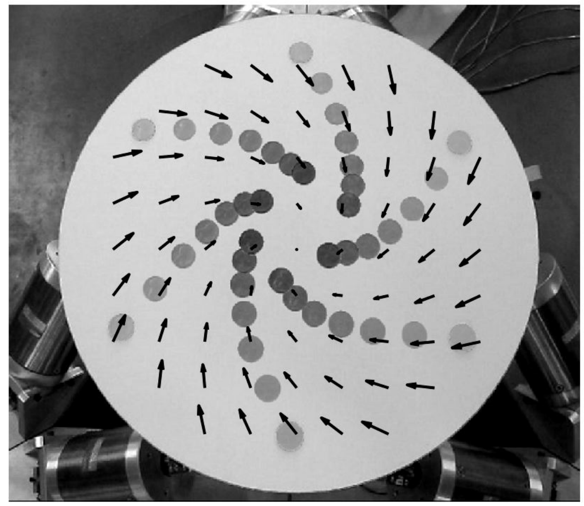

Fig. 1. A multi-exposure overhead image of six pennies moving in a `Whirlpool` field on the PPOD2 (Programmable Parts-feeding Oscillatory Device). The time interval between the images is 0.75 s. The overlaid vectors are numerically computed asymptotic velocities based on the plate's motion.

This work was supported by NSF grant CMMI-0700537 and Thomas Vose's NSF Graduate Research Fellowship.

T. H. Vose, P. Umbanhowar, and K. M. Lynch are with the Department of Mechanical Engineering, Northwestern University, Evanston, IL 60208 USA `{t-vose, umbanhowar, kmlynch}@northwestern.edu`

[1]Square wave accelerations are chosen because the asymptotic velocity fields they generate have closed-form solutions.

which the part does not stick or lose contact, and produces a unique point in a three-dimensional space $\mathcal{D}$. Given any point in $\mathcal{D}$, the second map Π_2 gives a unique scalar asymptotic velocity $\tilde{v} \in \mathbb{R}^1$. Given a scalar asymptotic velocity and the direction of the plate's in-plane motion component, the third map Π_3 gives the two-dimensional asymptotic velocity at $\tilde{\mathbf{r}}_{xy}$ in the field generated by M. The field $F \in \mathcal{F}$ is constructed by applying these three maps for all $\tilde{\mathbf{r}}_{xy} \in \mathcal{R}^M$.

II. BACKGROUND

Using programmable force fields to drive planar parts to stable equilibrium configurations without sensing is a well-studied topic [2], [3], [4], [5], [6]. Using a single rigid vibrating plate to program friction-induced versions of these fields is appealing because the resulting fields are continuous and the plate can be driven with few actuators. This is in contrast to array-based systems (e.g., [7], [8], [9]) which produce discrete fields and require many actuators.

Most previously studied vibratory systems have three or fewer degrees of freedom. One- and two-DoF translating plates can only generate translational fields [10], [11], [12], [13]. Adding a rotational freedom to the plate creates more possibilities. Examples include two-DoF [14] and three-DoF [15], [16] plates that can generate fields to position and orient parts with feedback from vision sensors, and a two-DoF plate [17] that can generate squeeze fields for sensorless positioning and orienting. This paper extends our previous work to determine what further types of fields are obtainable with a six-DoF plate, particularly for sensorless applications [1], [18].

III. SYSTEM MODEL

A. Plate Kinematics

Consider a rigid plate undergoing small-amplitude vibration. All subsequent vectors are defined with respect to a fixed inertial frame $\mathcal{W}$. In the *home position* the origin of $\mathcal{W}$ coincides with the center of mass of the plate. The z-axis of $\mathcal{W}$ is in the direction opposite the gravity vector $\mathbf{g} = [0, 0, -g]^T$, $g > 0$. The configuration of the plate is given by $(\mathbf{R}, \mathbf{p})$, where $\mathbf{R} \in SO(3)$ and $\mathbf{p} \in \mathbb{R}^3$. Both $\mathbf{R}$ and $\mathbf{p}$ are periodic C^1 functions of time with period T. In the home position, $\mathbf{p} = \mathbf{0}$ and $\mathbf{R} = \mathbf{I}$, where $\mathbf{I}$ is the identity matrix. The linear velocity of the origin of the plate is $\dot{\mathbf{p}} = [\dot{p}_x, \dot{p}_y, \dot{p}_z]^T$ and the angular velocity of the plate is $\boldsymbol{\omega} = [\omega_x, \omega_y, \omega_z]^T$. The linear acceleration of the origin of the plate is $\ddot{\mathbf{p}} = [\ddot{p}_x, \ddot{p}_y, \ddot{p}_z]^T$ and the angular acceleration of the plate is $\boldsymbol{\alpha} = [\alpha_x, \alpha_y, \alpha_z]^T$.

In this paper, we analyze plate motions $\mathcal{M}$ that combine a single in-plane acceleration component ($\ddot{p}_x$, $\ddot{p}_y$, or α_z) with a single out-of-plane acceleration component ($\ddot{p}_z$, α_x, or α_y). Each of the nine possible combinations (see Table I) is referred to as a *basic* plate motion. Both the in-plane and out-of-plane acceleration components are modeled as square waves with period T. Mathematically, we define the in-plane components as

$$\ddot{p}_x(t) = \begin{cases} A_x & 0 \le t < T/2 \\ -A_x & T/2 \le t < T \end{cases} \tag{1}$$

$$\ddot{p}_y(t) = \begin{cases} A_y & 0 \le t < T/2 \\ -A_y & T/2 \le t < T \end{cases} \tag{2}$$

$$\alpha_z(t) = \begin{cases} A_{\psi_z} & 0 \le t < T/2 \\ -A_{\psi_z} & T/2 \le t < T, \end{cases} \tag{3}$$

and the out-of-plane components as

$$\ddot{p}_z(t) = \begin{cases} -A_z & 0 \le t < \tau \\ A_z & \tau \le t < \tau + T/2 \\ -A_z & \tau + T/2 \le t < T \end{cases} \tag{4}$$

$$\alpha_x(t) = \begin{cases} -A_{\psi_x} & 0 \le t < \tau \\ A_{\psi_x} & \tau \le t < \tau + T/2 \\ -A_{\psi_x} & \tau + T/2 \le t < T \end{cases} \tag{5}$$

$$\alpha_y(t) = \begin{cases} -A_{\psi_y} & 0 \le t < \tau \\ A_{\psi_y} & \tau \le t < \tau + T/2 \\ -A_{\psi_y} & \tau + T/2 \le t < T, \end{cases} \tag{6}$$

where A_x, A_y, A_{ψ_z}, A_z, A_{ψ_x}, and A_{ψ_y} are positive constants and $0 \le \tau < T/2$ is a time corresponding to the relative phase between the in- and out-of-plane components. Formally, the space of basic plate motions is defined as $\mathcal{M} = \{(A_o, A_i, T, \tau, o, i)\} \subset \mathbb{R}^4 \times \mathcal{O} \times \mathcal{I}$, where $o \in \mathcal{O} = \{\text{“}z\text{”}, \text{“}\psi_x\text{”}, \text{“}\psi_y\text{”}\}$ and $i \in \mathcal{I} = \{\text{“}x\text{”}, \text{“}y\text{”}, \text{“}\psi_z\text{”}\}$ specify the out-of-plane and in-plane motion directions.

B. Part Dynamics

As in previous work [1], we assume that the part is sliding at all times and that its Coriolis and centripetal accelerations are insignificant. We also assume that linear and angular displacements of the plate are small enough that $\mathbf{p} \approx \mathbf{0}$ and $\mathbf{R} \approx \mathbf{I}$. It follows that the gravitational and normal forces are approximately aligned with the axes of $\mathcal{W}$ and that the part's position $\mathbf{r}$ in $\mathcal{W}$ is $\mathbf{r} \approx \mathbf{r}_{xy} = [x, y, 0]^T$ in Cartesian coordinates or $\mathbf{r} \approx \mathbf{r}_{r\theta} = [r, \theta, 0]^T$ in cylindrical coordinates. The approximate in-plane acceleration $\mathbf{a}_{xy}$ of the part is

$$\mathbf{a}_{xy} = [\ddot{x}, \ddot{y}, 0]^T \approx -\mu g_{\text{eff}} \frac{\dot{\mathbf{q}}}{\|\dot{\mathbf{q}}\|}, \tag{7}$$

where μ is the kinetic friction coefficient, g_{eff} is the effective gravity

$$g_{\text{eff}} \approx \ddot{p}_z + \alpha_x y - \alpha_y x + g, \tag{8}$$

and $\dot{\mathbf{q}}$ is the relative velocity between the part and the plate

$$\dot{\mathbf{q}} \approx [\dot{x} - (\dot{p}_x - \omega_z y), \dot{y} - (\dot{p}_y + \omega_z x), 0]^T. \tag{9}$$

From (7) and (8), the magnitude of $\mathbf{a}_{xy}$ is set by the plate's out-of-plane acceleration (i.e., g_{eff}). For a basic plate motion the magnitude of $\mathbf{a}_{xy}$ at a fixed location $\mathbf{r}$ must be one of two discrete values due to the form of (4)–(6). From (7) and (9), the direction of $\mathbf{a}_{xy}$ is set by the relative in-plane velocities of the part and the plate (i.e., $\dot{\mathbf{q}}$). Thus, for any basic plate

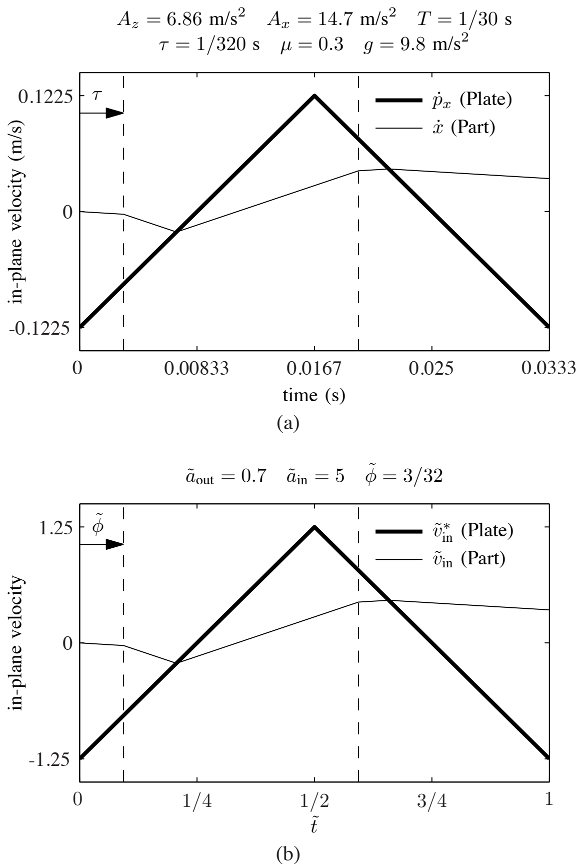

Fig. 2. (a) In-plane velocity trajectories of the part and the plate for one cycle of a basic plate motion combining $\ddot{p}_x$ and $\ddot{p}_z$. These trajectories are based on the plate motion $M = (6.86\,\text{m/s}^2, 14.7\,\text{m/s}^2, 1/30\,\text{s}, 1/320\,\text{s}, \text{“}z\text{”}, \text{“}x\text{”}) \in \mathcal{M}$ at position $\tilde{\mathbf{r}}_{xy} = (0,0)$, with $\mu = 0.3$ and $g = 9.8\,\text{m/s}^2$. (b) The same trajectories are shown in dimensionless form. For any plate motion in $\mathcal{M}$, all locations on the plate's surface for which $\tilde{a}_{\text{out}} = 0.7$, $\tilde{a}_{\text{in}} = 5$, and $\tilde{\phi} = 1/8$ will generate identical trajectories to those in (b) for the same initial condition. For the initial condition shown ($\tilde{v}_{\text{in}}(0) = 0$), the part is not in an asymptotic cycle since $\tilde{v}_{\text{in}}(0) \neq \tilde{v}_{\text{in}}(1)$.

motion, a part starting from rest must always move in the direction defined by the plate's in-plane motion component.

As an example, consider the basic plate motion combining the motion directions “z” and “x”. Fig. 2(a) shows the in-plane velocities of the plate $\dot{p}_x$ and the part $\dot{x}$ at location $\mathbf{r} = (0,0)$ as functions of time for one cycle of plate motion, assuming a negligible change in the part's position during the cycle. The slope of $\dot{p}_x$ corresponds to $\ddot{p}_x$, which from (1) is equal to $\pm A_x$. The slope of $\dot{x}$ corresponds to $\mathbf{a}_{xy}$ given by (7). From (8) the magnitude of the slope of $\dot{x}$ has a constant value of $\mu(-A_z + g)$ for $0 \leq t < \tau$ and $\tau + T/2 \leq t < T$, and a constant value of $\mu(A_z + g)$ for $\tau \leq t < \tau + T/2$. From (9) the slope of $\dot{x}$ is negative when $\dot{x} > \dot{p}_x$ and positive when $\dot{x} < \dot{p}_x$.

C. Non-dimensionalizing the System

For each of the nine basic plate motions we define a dimensionless out-of-plane plate acceleration $\tilde{a}_{\text{out}}$, a dimensionless in-plane plate acceleration $\tilde{a}_{\text{in}}$, a dimensionless phase $\tilde{\phi}$, and a dimensionless position on the plate surface in either Cartesian $\tilde{\mathbf{r}}_{xy} = (\tilde{x}, \tilde{y})$ or polar $\tilde{\mathbf{r}}_{r\theta} = (\tilde{r}, \tilde{\theta})$ coordinates (see Table I for defintions)[2]. Additionally, we define a dimensionless in-plane part velocity $\tilde{v}_{\text{in}} = \dot{x}/(\mu g T)$, and a dimensionless in-plane plate velocity $\tilde{v}^*_{\text{in}} = \dot{p}_x/(\mu g T)$. Finally, we non-dimensionalize time variables by dividing them by T (i.e., $\tilde{t} = t/T$).

The in-plane velocity trajectories shown in Fig. 2(a) transform into those shown in Fig. 2(b) when expressed dimensionlessly. The advantage of this dimensionless formulation is that it allows us to map any plate motion in $\mathcal{M}$ and a position on the plate surface to a single point $(\tilde{a}_{\text{out}}, \tilde{a}_{\text{in}}, \tilde{\phi})$ in a three-dimensional space. We can then associate the time trajectories for $\tilde{v}_{\text{in}}$ and $\tilde{v}^*_{\text{in}}$ with this point and not worry about the particular plate motion and location to which they actually correspond.

D. Asymptotic Velocity

If a point part is located at $\tilde{\mathbf{r}}_{xy}$ and its change in position is assumed to be negligible throughout the cycle, then the magnitude of the difference between its velocity at the beginning and end of the cycle is guaranteed to decrease every cycle [1]. Consequently, $\tilde{v}_{\text{in}}$ converges to a periodic cycle with period $\tilde{T} = 1$. We refer to such a cycle as an *asymptotic cycle*. We define the asymptotic velocity $\tilde{v}$ as the part's average velocity in an asymptotic cycle:

$$\tilde{v} = \int_0^1 \tilde{v}_{\text{in}}(\tilde{t})\,d\tilde{t}. \tag{10}$$

For basic plate motions, the direction of $\tilde{v}_{\text{in}}$ must converge to the plate's in-plane motion direction [1]. Thus, $\tilde{v}$ is a *scalar* asymptotic velocity for all plate motions in $\mathcal{M}$.

The rate of convergence to an asymptotic cycle depends on the part's position, the plate's motion, and the friction coefficient. We will assume the rate of convergence is always large enough to ensure that the asymptotic velocity approximates the part's true motion. Results in [1], [18], [19] provide experimental and simulation-based justification for this assumption.

IV. THE THREE MAPS

We define the three-dimensional set $\mathcal{D} = \{(\tilde{a}_{\text{out}}, \tilde{a}_{\text{in}}, \tilde{\phi}) : |\tilde{a}_{\text{out}}| < 1, \tilde{a}_{\text{in}} > 1 + |\tilde{a}_{\text{out}}|, 0 \leq \tilde{\phi} < 1/2\}$. The constraint $|\tilde{a}_{\text{out}}| < 1$ ensures the part never loses contact with the plate; the constraint $\tilde{a}_{\text{in}} > 1 + |\tilde{a}_{\text{out}}|$ ensures the part never sticks to the plate; the constraint $0 \leq \tilde{\phi} < 1/2$ is motivated by a symmetry of asymptotic velocities discussed in [17]: $\tilde{v}(\tilde{a}_{\text{out}}, \tilde{a}_{\text{in}}, \tilde{\phi} + 1/2) = \tilde{v}(-\tilde{a}_{\text{out}}, \tilde{a}_{\text{in}}, \tilde{\phi})$. We also define the set $\mathcal{R}^M$ as all positions $\tilde{\mathbf{r}}_{xy}$ that satisfy the constraints above for the basic plate motion $M \in \mathcal{M}$. Using Table I, we can construct a map Π_1 which converts M and $\tilde{\mathbf{r}}_{xy} \in \mathcal{R}^M$ to an element of $\mathcal{D}$: $\Pi_1 : \mathcal{M} \times \mathcal{R}^M \rightarrow \mathcal{D}$. Applying this map to all $\tilde{\mathbf{r}}_{xy} \in \mathcal{R}^M$ yields a simply-connected subset of $\mathcal{D}$ corresponding to M.

[2] $\tilde{x}$ and $\tilde{y}$ for the first two basic plate motions (columns) in Table I are non-dimensionalized with respect to an arbitrary length scale ℓ_0 because fields generated by these plate motions are translationally invariant (i.e., there is no natural length scale).

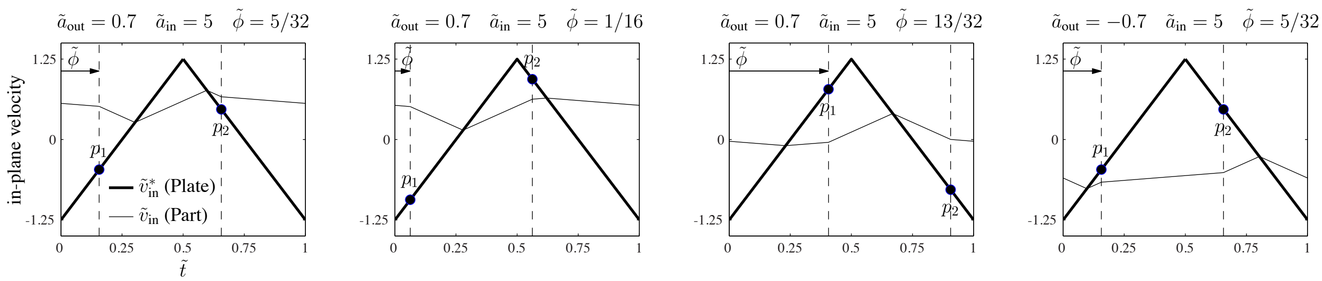

(a) AA cycle (b) AB cycle (c) BA cycle (d) BB cycle

Fig. 3. Examples of the four pure asymptotic cycles. Note that $\tilde{v}_{\text{in}}(0) = \tilde{v}_{\text{in}}(1)$.

TABLE I

	Trans	Trans	Circle	NodalLine	NodalLine	NodalLine	NodalLine	DivCircle	DivCircle
o	"z"	"z"	"z"	"ψ_y"	"ψ_x"	"ψ_x"	"ψ_y"	"ψ_z"	"ψ_z"
i	"x"	"y"	"ψ_z"	"x"	"y"	"x"	"y"	"ψ_x"	"ψ_y"
$\tilde{a}_{\text{out}}$	$\frac{A_z}{g}$	$\frac{A_z}{g}$	$\frac{A_z}{g}$	$\frac{A_{\psi_y}}{g}x$	$\frac{A_{\psi_x}}{g}y$	$\frac{A_{\psi_x}}{g}y$	$\frac{A_{\psi_y}}{g}x$	$\frac{A_{\psi_x}}{g}r\sin\theta$	$\frac{A_{\psi_y}}{g}r\cos\theta$
$\tilde{a}_{\text{in}}$	$\frac{A_x}{\mu g}$	$\frac{A_y}{\mu g}$	$\frac{A_{\psi_z}}{\mu g}r$	$\frac{A_x}{\mu g}$	$\frac{A_y}{\mu g}$	$\frac{A_x}{\mu g}$	$\frac{A_y}{\mu g}$	$\frac{A_{\psi_z}}{\mu g}r$	$\frac{A_{\psi_z}}{\mu g}r$
$\tilde{\phi}$	$\frac{\tau}{T}$	$\frac{\tau}{T}$	$\frac{\tau}{T}$	$\frac{\tau}{T}$	$\frac{\tau}{T}$	$\frac{\tau}{T}$	$\frac{\tau}{T}$	$\frac{\tau}{T}$	$\frac{\tau}{T}$
$\tilde{x}$ or $\tilde{r}$	$\frac{1}{\ell_0}x$	$\frac{1}{\ell_0}x$	$\frac{A_{\psi_z}}{g}r$	$\frac{A_{\psi_y}}{g}x$	$\frac{A_{\psi_x}}{g}x$	$\frac{A_{\psi_x}}{g}x$	$\frac{A_{\psi_y}}{g}x$	$\frac{A_{\psi_x}}{g}r$	$\frac{A_{\psi_y}}{g}r$
$\tilde{y}$ or $\tilde{\theta}$	$\frac{1}{\ell_0}y$	$\frac{1}{\ell_0}y$	θ	$\frac{A_{\psi_y}}{g}y$	$\frac{A_{\psi_x}}{g}y$	$\frac{A_{\psi_x}}{g}y$	$\frac{A_{\psi_y}}{g}y$	θ	θ

For any M, there are exactly nine types of asymptotic cycles to which $\tilde{v}_{\text{in}}$ can potentially converge. Four of the nine, which are shown in Fig. 3, are referred to as *pure cycles*, and are classified as AA, AB, BA, or BB. This classification indicates whether $\tilde{v}_{\text{in}}$ passes above (A) or below (B) the points p_1 and p_2, where p_1 is the point on $\tilde{v}_{\text{in}}^*$ at $\tilde{t} = \tilde{\phi}$ and p_2 is the point on $\tilde{v}_{\text{in}}^*$ at $\tilde{t} = \tilde{\phi} + 1/2$. The other five types of cycles occur when $\tilde{v}_{\text{in}}$ passes directly through p_1 (TA and TB cycles), directly through p_2 (AT and BT cycles), or directly through both p_1 and p_2 (TT cycles). We refer to these five as *transition cycles* because they must be transitioned through to get from one type of pure cycle to another. For each of the nine cycle types there is a closed-form solution (see [17]) to (10) that gives a unique scalar asymptotic velocity as a function of the triple $(\tilde{a}_{\text{out}}, \tilde{a}_{\text{in}}, \tilde{\phi}) \in \mathcal{D}$. Thus, (10) is equivalent to the map $\Pi_2 : \mathcal{D} \rightarrow V$, where $V = \mathbb{R}^1$.

A representation of $\mathcal{D}$ is shown in Fig. 4. There are four three-dimensional subsets of $\mathcal{D}$ denoted AA, AB, BA, BB that correspond to points with those respective pure cycles. These four subsets are separated by four two-dimensional *transition surfaces* AT, TA, BT, TB corresponding points with those respective transition cycles, and a one-dimensional transition line TT corresponding to points with TT cycles. To help visualize the map Π_2, the surfaces in Fig. 4 are shaded according to their asymptotic speed $|\tilde{v}|$ based on the analytic solutions to (10). It only appears that Π_2 has an even symmetry with respect to $\tilde{a}_{\text{out}}$ because the shading is based on $|\tilde{v}|$ and not $\tilde{v}$; in fact, the symmetry is odd: $\Pi_2(\tilde{a}_{\text{out}}, \tilde{a}_{\text{in}}, \tilde{\phi}) = -\Pi_2(-\tilde{a}_{\text{out}}, \tilde{a}_{\text{in}}, \tilde{\phi})$. The two-dimensional surface defined by the dashed boundary is not a transition surface but rather a *zero-velocity surface*—BA cycles just above and below this surface have scalar asymptotic velocities with opposite signs. All points below the zero-velocity surface with $\tilde{a}_{\text{out}} > 0$ ($\tilde{a}_{\text{out}} < 0$) map to positive (negative) scalar asymptotic velocities. All points above the zero-velocity surface with $\tilde{a}_{\text{out}} > 0$ ($\tilde{a}_{\text{out}} < 0$) map to negative (positive) scalar asymptotic velocities. Equations defining all of these subsets of $\mathcal{D}$ are given in [17].

Knowing the *scalar* asymptotic velocity at $\tilde{\mathbf{r}}_{xy}$ is not sufficient to determine the direction of the asymptotic velocity vector at $\tilde{\mathbf{r}}_{xy}$ in a field $F \in \mathcal{F}$. As previously discussed, however, a positive (negative) scalar asymptotic velocity indicates the asymptotic velocity vector at $\tilde{\mathbf{r}}_{xy}$ points in the positive (negative) direction of the plate's in-plane motion component, i. Thus, we define a third map, $\Pi_3 : V \times \mathcal{I} \rightarrow \mathcal{V}$, where $\mathcal{V}$ is the set of all two-dimensional asymptotic velocities that can be generated by plate motions in $\mathcal{M}$.

V. CONSTRUCTING FIELDS IN $\mathcal{F}$

By combining Π_1, Π_2, and Π_3 we can form the map $\Pi : \mathcal{M} \times \mathcal{R}^M \rightarrow \mathcal{V}$. For a particular plate motion M, we can apply Π to all $\tilde{\mathbf{r}}_{xy} \in \mathcal{R}^M$ and construct the corresponding asymptotic velocity field in $\mathcal{F}$. However, the key to understanding the structure of $\mathcal{F}$ is understanding the three individual maps. To illustrate, we devote the rest of this section to constructing a representative field for each basic plate motion. Due to the nature of Π_1 and Π_2, the particular plate motions we examine generate fields that are well approximated by polynomial functions of the part's position with degree $n \leq 2$.

A. *Trans Class: "z" + "x" and "z" + "y"*

Consider basic plate motions of the form $M = (A_z, A_x, \tau, \text{"}z\text{"}, \text{"}x\text{"})$, which generate fields in the Trans class. From the first column of Table I we see that Π_1 maps all $\tilde{\mathbf{r}}_{xy} \in \mathcal{R}^M$ for this M to a single point $d \in \mathcal{D}$. The mapping is represented graphically in Fig. 5. For the particular M generating the field in Fig. 5(a), the dashed and solid lines (and all other points in $\mathcal{R}^M$) map to the point $d = (0.5, 7, 3/8)$, which is shown in Fig. 5(c). Applying Π_2 to d gives the scalar asymptotic velocity for all $\tilde{\mathbf{r}}_{xy} \in \mathcal{R}^M$. Because i = "x", Π_3 dictates that the asymptotic velocity at each $\tilde{\mathbf{r}}_{xy}$ in the field must point in the x-direction. Thus, there is a set of fields in $\mathcal{F}$ of the form

$$\begin{bmatrix} \tilde{v}_{\tilde{x}} \\ \tilde{v}_{\tilde{y}} \end{bmatrix} = b \begin{bmatrix} 1 \\ 0 \end{bmatrix}, \tag{11}$$

where b is a constant that depends on $\tilde{a}_{\text{out}}$, $\tilde{a}_{\text{in}}$, and $\tilde{\phi}$. For the particular field shown in Fig. 5(a), $b > 0$ because Π_2 maps d to a *positive* scalar asymptotic velocity (Fig. 5(c)).

Fields characterized by (11) share the basis $[1, 0]^T$ and are called `TransX` fields. The other basic plate motion associated with the Trans class generates a set of `TransY` fields that share the basis $[0, 1]^T$. Note that the `TransY` field in Fig. 5(b) and the `TransX` field in Fig. 5(a) both correspond to the same point $d \in \mathcal{D}$. More generally, all fields in the Trans class correspond to a zero-dimensional subset of $\mathcal{D}$ and have the same velocity at all $\tilde{\mathbf{r}}_{xy}$.

B. *Circle Class: "z" + "ψ_z"*

Basic plate motions of the form $M = (A_z, A_{\psi_z}, \tau, \text{"}z\text{"}, \text{"}\psi_z\text{"})$ generate fields in the Circle class. From the third column of Table I, $\tilde{a}_{\text{out}}$ and $\tilde{\phi}$ are constant for this M, but $\tilde{a}_{\text{in}}$ depends on $\tilde{r}$; specifically, $\tilde{a}_{\text{in}} = \tilde{r}/\mu$. Thus, Π_1 maps M and every set of points in $\mathcal{R}^M$ satisfying $\tilde{\theta} = \tilde{\theta}_0$ (e.g., the solid radial line in Fig. 6(a)) to a line in $\mathcal{D}$ parallel to the $\tilde{a}_{\text{in}}$ axis (Fig. 6(b)). Equivalently, Π_1 maps M and every set of points in $\mathcal{R}^M$ satisfying $\tilde{r} = \tilde{r}_0$ (e.g., the dashed circle in Fig. 6(a)) to a single point on the same line. For the particular M generating the field in Fig. 6(a), the line in $\mathcal{D}$ is described by $\tilde{a}_{\text{out}} = 0.5$ and $\tilde{\phi} = 5/32$. All points on this line correspond to AA cycles. Fig. 6(c) shows how Π_2 maps $\tilde{a}_{\text{in}}$ to $\tilde{v}$ along this line and illustrates a general property of Π_2: nearly all points corresponding to AA cycles get mapped such that $\tilde{v}$ is approximately proportional to $\tilde{a}_{\text{in}}$. Because i = "ψ_z", Π_3 dictates that the asymptotic velocity at each $\tilde{\mathbf{r}}_{r\theta}$ in the field must point in the ψ_z-direction (angular direction). Thus, there is a set fields in $\mathcal{F}$ with the form

$$\begin{bmatrix} \tilde{v}_{\tilde{r}} \\ \tilde{v}_{\tilde{\theta}} \end{bmatrix} \approx \frac{b}{\mu} \begin{bmatrix} 0 \\ \tilde{r} \end{bmatrix}, \tag{12}$$

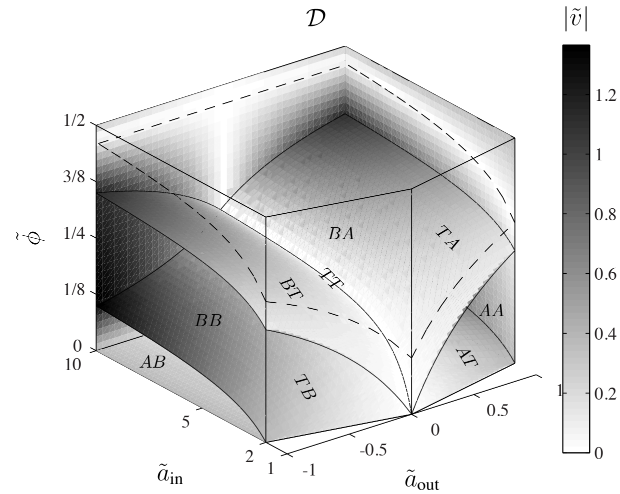

Fig. 4. The thee-dimensional space $\mathcal{D}$. AA, AB, BA, and BB are three-dimensional subsets corresponding to points with those respective pure cycles. AT, TA, BT, and TB are two-dimensional subsets corresponding to points with transition cycles that pass through either p_1 or p_2. TT is a one-dimensional subset corresponding to points with transition cycles that pass through p_1 and p_2. The BA subset also contains the two-dimensional zero-velocity surface whose boundary is shown dashed. Π_2 maps all points below the zero-velocity surface with $\tilde{a}_{\text{out}} < 0$ ($\tilde{a}_{\text{out}} > 0$) to positive (negative) scalar asymptotic velocities; it maps all points above the zero-velocity surface with $\tilde{a}_{\text{out}} < 0$ ($\tilde{a}_{\text{out}} > 0$) to negative (positive) asymptotic velocities. The shading corresponds to the asymptotic speed based on Π_2. Slices of $\mathcal{D}$ are shown in Figs. 5–8. Note that $\tilde{a}_{\text{in}} = 10$ is an arbitrary cutoff, not an actual boundary of $\mathcal{D}$.

where b is a constant that depends on $\tilde{a}_{\text{out}}$ and $\tilde{\phi}$. Fields characterized by (12) share the basis $[0, \tilde{r}]^T$ (in polar coordinates) and are called `Circle` fields.

All fields in the Circle class correspond to one-dimensional subsets of $\mathcal{D}$ parallel to the $\tilde{a}_{\text{in}}$ axis. If we had chosen a different M than the one corresponding to the field in Fig. 6(a), then the subset in $\mathcal{D}$ would differ from the one in Fig. 6(b). As a result, Π_2 may introduce a nonlinear relationship between $\tilde{a}_{\text{in}}$ and $\tilde{v}$. For example, if $\tilde{\phi} > 1/4$ then the subset in $\mathcal{D}$ includes a point on the zero-velocity surface (dashed line in Fig. 6(b)). This type of subset maps to fields with velocity vectors that switch from counterclockwise to clockwise at a critical radius. We also note that because $\tilde{a}_{\text{in}} > 1 + |\tilde{a}_{\text{out}}|$ is required to avoid sticking, there is a minimum radius $\tilde{r}_{\text{min}} = \mu(1 + \tilde{a}_{\text{out}})$ for all fields in the Circle class below which our analysis does not yield solutions.

C. *NodalLine Class: "ψ_y" + "x", "ψ_x" + "y", "ψ_x" + "x", and "ψ_y" + "y"*

Consider basic plate motions of the form $M = (A_{\psi_y}, A_x, \tau, \text{"}\psi_y\text{"}, \text{"}x\text{"})$, which generate fields in the the NodalLine class. From the fourth column of Table I, $\tilde{a}_{\text{in}}$ and $\tilde{\phi}$ are constant, but $\tilde{a}_{\text{out}}$ depends on $\tilde{x}$; specifically, $\tilde{a}_{\text{out}} = \tilde{x}$. Thus, Π_1 maps M and every set of points in $\mathcal{R}^M$ satisfying $\tilde{x} = \tilde{x}_0$ (e.g., the solid line in Fig. 7(a)) to a line in $\mathcal{D}$ parallel to the $\tilde{a}_{\text{out}}$ axis (Fig. 7(e)). Equivalently, Π_1 maps M and every set of points in $\mathcal{R}^M$ satisfying $\tilde{y} = \tilde{y}_0$ (e.g., the dashed line in Fig. 7(a)) to a single point on the same line. For the particular M generating the field in Fig. 7(a),

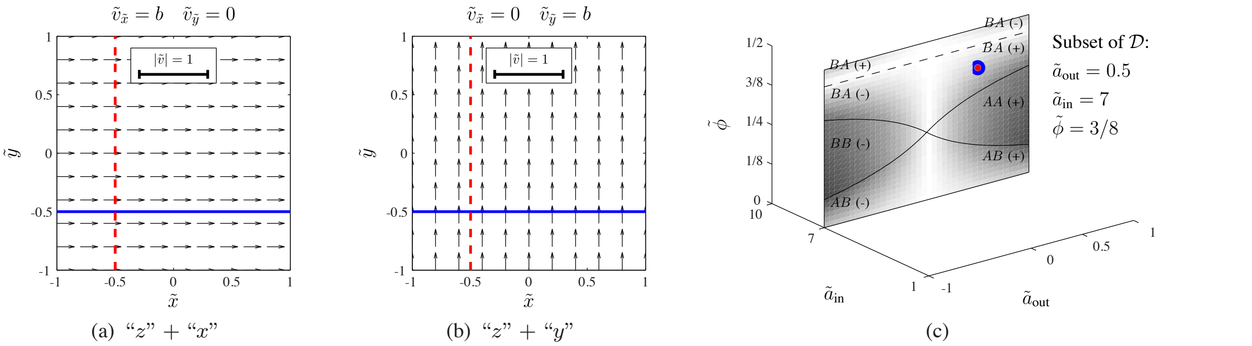

Fig. 5. The `TransX` and `TransY` fields in (a) and (b) correspond to the same zero-dimensional subset of $\mathcal{D}$ shown in (c). The plus and minus signs in (c) indicate whether the scalar asymptotic velocity is positive or negative. The lines in (c) denote where the transition (solid) and zero-velocity (dashed) surfaces cut through the slice of $\mathcal{D}$.

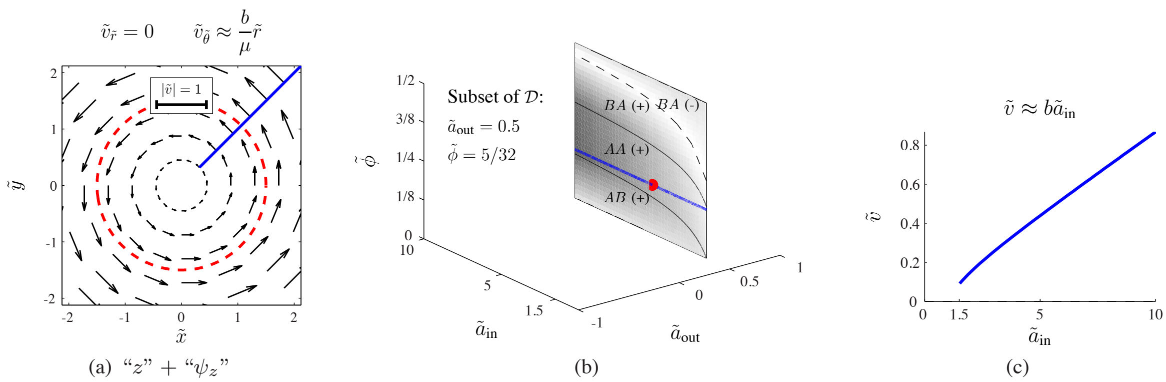

Fig. 6. The `Circle` field in (a) corresponds to the one-dimensional subset of $\mathcal{D}$ shown in (b). Because this subset is contained in the AA region, Π_2 maps points in it such that $\tilde{v}$ is approximately proportional to $\tilde{a}_{\text{in}}$ (c).

this line is described by $\tilde{a}_{\text{in}} = 7$ and $\tilde{\phi} = 1/16$. All points on this line correspond to AB cycles. Fig. 7(f) shows how Π_2 maps $\tilde{a}_{\text{in}}$ to $\tilde{v}$ along this line and illustrates a general property of Π_2: nearly all points corresponding to AB cycles get mapped such that $\tilde{v}$ is approximately proportional to $\tilde{a}_{\text{in}}$. Because $i =$ "x", Π_3 dictates that the asymptotic velocity at each $\tilde{\mathbf{r}}_{xy}$ in the field must point in the x-direction. Thus, there is a set fields in $\mathcal{F}$ with the form

$$\begin{bmatrix} \tilde{v}_{\tilde{x}} \\ \tilde{v}_{\tilde{y}} \end{bmatrix} \approx b \begin{bmatrix} \tilde{x} \\ 0 \end{bmatrix}, \tag{13}$$

where b is a constant that depends on $\tilde{a}_{\text{in}}$ and $\tilde{\phi}$. Fields characterized by (13) share the basis $[\tilde{x}, 0]^T$ and are called `NodalLineX` fields.

The three other basic plate motions associated with the NodalLine class generate a set of of `NodalLineY` fields with basis $[0, \tilde{y}]^T$, a set of `ShearX` fields with basis $[\tilde{y}, 0]^T$, and a set of `ShearY` fields with basis $[0, \tilde{x}]^T$. Examples of these fields are shown in Fig. 7(b)–(d). Note that all four fields in Fig. 7 correspond to the same subset of $\mathcal{D}$. Though all fields in the NodalLine class correspond to one-dimensional subsets of $\mathcal{D}$ parallel to the $\tilde{a}_{\text{out}}$ axis, not all exhibit a linear relationship between velocity and position.

D. DivCircle Class: "ψ_x" + "ψ_z" and "ψ_y" + "ψ_z"

Consider basic plate motions of the form $M = (A_{\psi_x}, A_{\psi_z}, \tau,$ "ψ_x", "ψ_z"$)$, which generate fields in the DivCircle class. From the eighth column of Table I, $\tilde{\phi}$ is constant, but $\tilde{a}_{\text{in}}$ depends on $\tilde{r}$, and $\tilde{a}_{\text{out}}$ depends on both $\tilde{r}$ and $\tilde{\theta}$; specifically, $\tilde{a}_{\text{out}} = \tilde{r}\sin\tilde{\theta}$, and $\tilde{a}_{\text{in}} = \tilde{m}\tilde{r}$, where $\tilde{m} = A_{\psi_z}/(\mu A_{\psi_x})$ is a dimensionless constant that determines the minimum distance $\tilde{r}_{\text{min}} = 1/(\tilde{m} - |\sin\tilde{\theta}|)$ the part can be from the origin without sticking.

Π_1 maps M and every set of points in $\mathcal{R}^M$ satisfying $\tilde{r} = \tilde{r}_0$ (e.g., the dashed semi-circles in Fig. 8(a)) to lines in $\mathcal{D}$ (the dashed lines in Fig. 8(c)) defined by $\tilde{a}_{\text{in}} = \tilde{m}\tilde{r}_0$ and $-\tilde{k} < \tilde{a}_{\text{out}} < \tilde{k}$, where k is the minimum of $\tilde{r}$, $\tilde{m}\tilde{r} - 1$, and 1. Π_1 maps M and every set of points in $\mathcal{R}^M$ satisfying $\tilde{\theta} = \tilde{\theta}_0$ (e.g., the solid radial lines in Fig. 8(a)) to lines in $\mathcal{D}$ defined by $\tilde{a}_{\text{in}} = (\tilde{m}/\sin\tilde{\theta}_0)\tilde{a}_{\text{out}}$ (the solid lines in Fig. 8(c)). Thus, Π_1 maps M and all $\tilde{\mathbf{r}}_{xy} \in \mathcal{R}^M$ to a horizontal plane in $\mathcal{D}$ with the constraint $\tilde{a}_{\text{in}} > \tilde{m}|\tilde{a}_{\text{out}}|$. For the particular M generating the field in Fig. 8(a), this plane is described by $\tilde{\phi} = 1/16$, $\tilde{a}_{\text{in}} > 5|\tilde{a}_{\text{out}}|$. Nearly all points in this plane correspond to AB cycles. Fig. 8(d) shows how Π_2 maps $\tilde{a}_{\text{out}}$ to $\tilde{v}$ along the dashed lines in this plane; Fig. 8(e) shows how Π_2 maps $\tilde{\rho}$ to $\tilde{v}$ along the solid lines in this plane (where $(\tilde{\rho}, \tilde{\gamma}, \tilde{\phi})$ is a point in $\mathcal{D}$ expressed in cylindrical coordinates). This illustrates a general property of Π_2: nearly all points corresponding to AB cycles are mapped such that $\tilde{v}$ is approximately proportional to both $\tilde{a}_{\text{out}}$ and $\tilde{a}_{\text{in}}$, or equivalently, $\tilde{v}$ is approximately proportional to both $\tilde{\rho}^2$ and $\sin\gamma\cos\gamma$ (Figs. 8(d) and (e)). Because $i =$ "ψ_z",

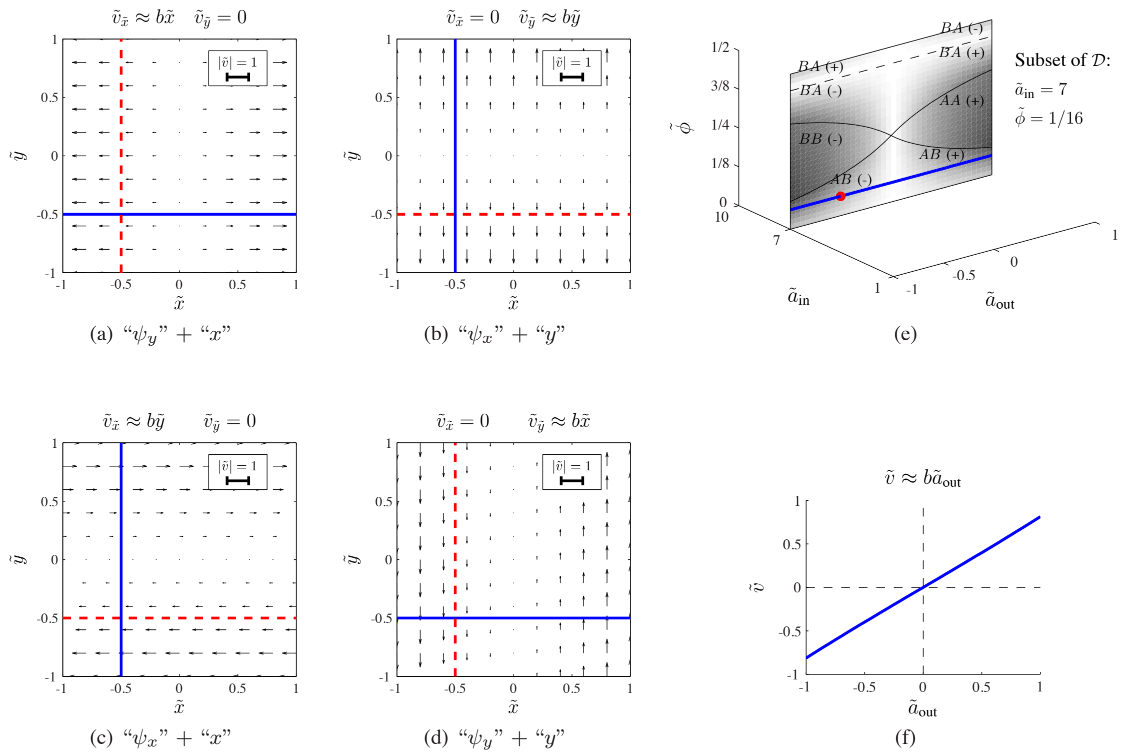

Fig. 7. The `NodalLineX`, `NodalLineY`, `ShearX`, and `ShearY` fields in (a)–(d) correspond to the same one-dimensional subset of $\mathcal{D}$ shown in (e). Because this subset is contained in the AB region, Π_2 maps points in it such that $\tilde{v}$ is approximately proportional to $\tilde{a}_{\text{out}}$ (f).

Π_3 dictates that the asymptotic velocity at each $\tilde{\mathbf{r}}_{r\theta}$ in the field must point in the ψ_z-direction (angular direction). Thus, there is a set of fields in $\mathcal{F}$ with the form

$$\begin{bmatrix} \tilde{v}_{\tilde{r}} \\ \tilde{v}_{\tilde{\theta}} \end{bmatrix} \approx b\tilde{m} \begin{bmatrix} 0 \\ \tilde{r}^2 \sin\tilde{\theta} \end{bmatrix}, \tag{14}$$

where b is a constant that depends on $\tilde{\phi}$. Fields characterized by (14) share the basis $[0, \tilde{r}^2 \sin\tilde{\theta}]^T$ (in polar coordinates) and are called `DivCircleX` fields. The other basic plate motion associated with the DivCircle class generates a set of `DivCircleY` fields with basis $[0, \tilde{r}^2 \cos\tilde{\theta}]^T$. The `DivCircleY` field in Fig. 8(b) and the `DivCircleX` field in Fig. 8(a) both correspond to the same subset of $\mathcal{D}$.

Though all fields in the DivCircle class correspond to subsets of $\mathcal{D}$ that are horizontal planes, not all are characterized by (14). For example, if the plate motion corresponds to $\tilde{\phi} > 5/16$, then the subset of $\mathcal{D}$ includes points on the zero-velocity surface. This type of subset maps to fields with velocity vectors that switch from counterclockwise to clockwise at a critical radius.

VI. Combining Fields in $\mathcal{F}$

When expressed in Cartesian coordinates, linear combinations of the nine basis fields presented in Section V form an eight-dimensional space of polynomial functions of position with degree $n \leq 2$:

$$\begin{aligned} \tilde{v}_{\tilde{x}} &= a_1\tilde{y}^2 + a_2\tilde{x}\tilde{y} + b_1\tilde{x} + b_2\tilde{y} + c_1 \\ \tilde{v}_{\tilde{y}} &= a_2\tilde{x}^2 + a_1\tilde{x}\tilde{y} + b_3\tilde{x} + b_4\tilde{y} + c_2, \end{aligned} \tag{15}$$

where $[a_1, a_2, b_1, b_2, b_3, b_4, c_1, c_2]^T$ is a full-dimensional subset of $\mathbb{R}^8$ that includes the origin.

Based on numerical simulations, we hypothesize that all fields in (15) can be generated by adding more motion components to a basic plate motion (such that all components have the same period and square wave accelerations). For example, the `Sink` field in Fig. 9 is a linear combination of a `NodalLineX` and a `NodalLineY` field. Using a gradient-based numerical optimization algorithm, one plate motion found to generate this `Sink` field (see Fig. 9) combines *two* in-plane motion components ("x" and "y") with *two* out-of-plane motion components ("ψ_x" and "ψ_y"). We note that this plate motion is parameterized by four amplitudes and *three* relative phases (between "x" and "ψ_y", "x" and "ψ_x", and "x" and "y"). Thus, the plate motion is *not* a strict sum of the plate motions used to generate the individual `NodalLineX` and `NodalLineY` fields—that motion has only two relative phases (between "x" and "ψ_y" and between "y" and "ψ_x").

VII. Conclusions

By deconstructing the map $\Pi : \mathcal{M} \rightarrow \mathcal{F}$ into three simpler maps, we have shown how to find all fields generated by plate motions in $\mathcal{M}$. The deconstruction also exposed how the relationship between $\mathcal{M}$ and $\mathcal{F}$ critically depends on simply-connected subsets of the three-dimensional space $\mathcal{D}$. The examples in Section V showed that many fields in $\mathcal{F}$ are well approximated by polynomial functions of position with degree $n \leq 2$. There is strong numerical evience that the fields in $\mathcal{F}$ approximately span the set of fields that can

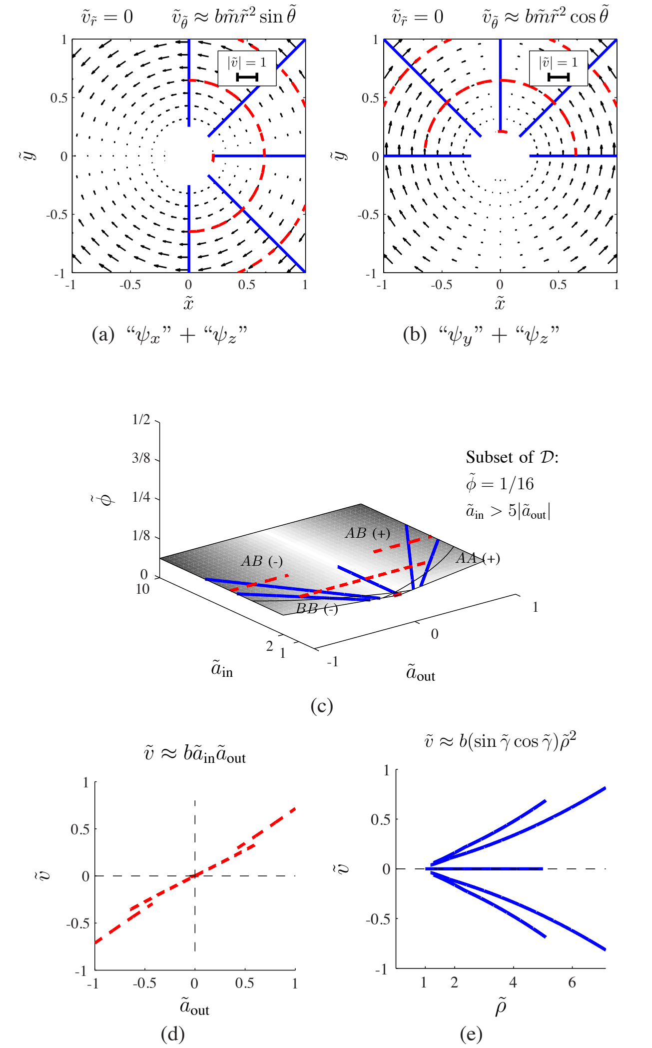

Fig. 8. The `DivCircleX` and `DivCircleY` fields in (a) and (b) correspond to the same two-dimensional subset of $\mathcal{D}$ shown in (c). Because this subset is almost entirely contained in the AB region, Π_2 maps points in it such that $\tilde{v}$ is approximately proportional to both $\tilde{a}_{\text{in}}$ and $\tilde{a}_{\text{out}}$ (d), or equivalently, $\tilde{v}$ is approximately proportional to both $\sin\tilde{\gamma}\cos\tilde{\gamma}$ and $\tilde{\rho}^2$ (e).

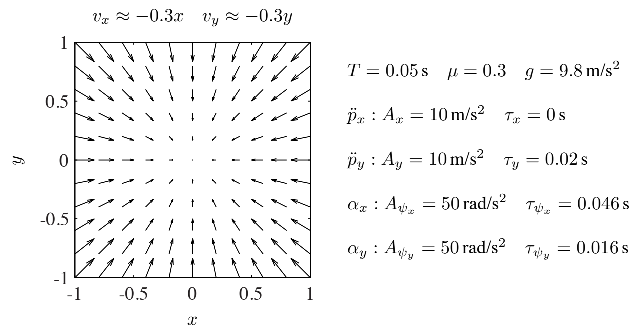

Fig. 9. A `Sink` field generated from a plate motion combining square wave accelerations for $\ddot{p}_x$, $\ddot{p}_y$, α_x, and α_y.

be generated from any plate motion whose six components have square, triangle, or sinusoidal accelerations with the same period; however, this is an area of future research. Additionally, we are investigating analogues of the three maps described in this paper for plate motions combining in-plane and out-of-plane components with different periods. By pairing components with different periods, we hope to build up a more complete understanding of the set of all fields that a six-DoF rigid plate can generate.

REFERENCES

[1] Thomas H. Vose, Paul Umbanhowar, and Kevin M. Lynch. Friction-induced velocity fields for point parts sliding on a rigid oscillated plate. *International Journal of Robotics Research*, 28(8):1020–1039, 2009.

[2] K.-F. Böhringer, L. Kavraki, and F. Lamiraux. Part orientation with one or two stable equilibria using programmable force fields. *IEEE Trans. Robot. Autom.*, 16:157–170, Apr 2000.

[3] K.-F. Böhringer, V. Bhatt, Bruce R. Donald, and K. Y. Goldberg. Algorithms for sensorless manipulation using a vibrating surface. *Algorithmica*, 16:389–429, 2000.

[4] A. Sudsang. Sensorless sorting of two parts in the plane using programmable force fields. In *IEEE International Conference on Intelligent Robots and Systems*, pages 1784–1789, 2002.

[5] F. Lamiraux and L. Kavraki. Positioning symmetric and non-symmetric parts using radial and constant force fields. In *Workshop on the Algorithmic Foundations of Robotics*, 2000.

[6] M.G. Coutinho and P.M. Will. A general theory for positioning and orienting 2d polygonal or curved parts using intelligent motion surfaces. In *IEEE International Conference on Robotics and Automation*, pages 856–862, 1998.

[7] J. E. Luntz, W. Messner, and H. Choset. Distributed manipulation using discrete actuator arrays. *International Journal of Robotics Research*, 20(7), July 2001.

[8] K.-F. Böhringer, B. R. Donald, and N. C. MacDonald. Programmable vector fields for distributed manipulation, with applications to MEMS actuator arrays and vibratory parts feeders. *International Journal of Robotics Research*, 18(2):168–200, Feb 1999.

[9] Peter U. Frei, Markus Wiesendanger, Roland Büchi, and Lorenz Ruf. Simultaneous planar transport of multiple objects on individual trajectories using friction forces. In Karl F. Böhringer and Howie Choset, editors, *Distributed Manipulation*, pages 49–64. Kluwer Academic Publishers, 2000.

[10] S. Okabe, Y. Kamiya, K. Tsujikado, and Y. Yokoyama. Vibratory feeding by nonsinusoidal vibration—optimum wave form. *ASME Journal of Vibration, Acoustics, Stress, and Reliability in Design*, 107:188–195, April 1985.

[11] W. A. Morcos. On the design of oscillating conveyers—case of simultaneous normal and longitudinal oscillations. *ASME Journal of Engineering for Industry*, 92(1):53–61, 1970.

[12] D. Reznik and J. Canny. The Coulomb pump: a novel parts feeding method using a horizontally-vibrating surface. In *IEEE International Conference on Robotics and Automation*, pages 869–874, 1998.

[13] Paul Umbanhowar and Kevin M. Lynch. Optimal vibratory stick-slip transport. *IEEE Transactions on Automation Science and Engineering*, 5(3):537–544, 2008.

[14] M. Higashimori, K. Utsumi, Y. Omoto, and M. Kaneko. Dynamic manipulation inspired by the handling of a pizza peel. In *IEEE Transactions on Robotics*, volume 25, pages 829–838, 2009.

[15] D. Reznik and J. Canny. A flat rigid plate is a universal planar manipulator. In *IEEE International Conference on Robotics and Automation*, pages 1471–1477, 1998.

[16] D. Reznik and J. Canny. C'mon part, do the local motion! In *IEEE International Conference on Robotics and Automation*, pages 2235–2242, 2001.

[17] Thomas H. Vose, Paul Umbanhowar, and Kevin M. Lynch. Friction-induced lines of attraction and repulsion for parts sliding on an oscillated plate. *IEEE Transactions on Automation Science and Engineering*, 6:685–699, 2009.

[18] Thomas H. Vose, Paul Umbanhowar, and Kevin M. Lynch. Vibration-induced frictional force fields on a rigid plate. In *IEEE International Conference on Robotics and Automation*, 2007.

[19] Stephen Berard, Binh Nguyen, Kurt Anderson, and J.C. Trinkle. Sources of error in a simulation of rigid parts on a vibrating rigid plate. In *ACM Symposium on Applied Computing*, pages 1181–1185, 2009.